Ferroelectrics

ISSN: (Print) (Online) Journal homepage: www.tandfonline.com/journals/gfer20

Dielectric analysis of surface modified nano-graphite: effects of frequency and thickness

Bhanu Pratap Singh, Pushpendra Kumar & S. P. Mahapatra

To cite this article: Bhanu Pratap Singh, Pushpendra Kumar & S. P. Mahapatra (2023) Dielectric analysis of surface modified nano-graphite: effects of frequency and thickness, Ferroelectrics, 617:1, 51-61, DOI: 10.1080/00150193.2023.2271133

To link to this article: https://doi.org/10.1080/00150193.2023.2271133

FERROELECTRICS
2023, VOL. 617, 51–61
https://doi.org/10.1080/00150193.2023.2271133

Taylor & Francis
Taylor & Francis Group

Dielectric analysis of surface modified nano-graphite: effects of frequency and thickness

Bhanu Pratap Singh, Pushpendra Kumar, and S. P. Mahapatra

Department of Chemistry, National Institute of Technology, Raipur, India

ABSTRACT

The nano-graphite (NG) and acid modified nano-graphite (ANG) have been synthesized from graphite powder via mixture of strong acid (sulphuric acid and nitric acid) respectively by a soft chemistry route involving microwave, ultrasonic method and characterized by high-resolution electron microscopy (HR-TEM), scanning electron microscopy (SEM), fourier-transform infrared spectroscopy (FTIR) and X-ray diffraction (XRD), clearly demonstrated the successful synthesis of acid modified NG. SEM images confirmed the surface morphology of NG, and ANG and HR-TEM study shows the nanoparticles size of NG and ANG. FTIR data confirmed the presence of acid functional groups on the surface of synthesized NG powder. XRD data of NG and ANG shows that 2θ is at 26.43° and 0.336 nm is an interlayer distance (d). NG and ANG pellets have been prepared for their dielectric analysis with frequency for different thickness. The dielectric loss tangent ($\tan\delta$) spectra show relaxation peak with frequency and peak shifts due to presence of polar groups in the ANG. The capacitance values of NG and ANG decrease with frequency and increase with thicknesses due to the capacitive nature of nanoparticles. The dielectric permittivity decreases with frequency and increases with thickness due to the charge orientation and dipole moment change of functional groups of synthesized NG, and ANG. The electrical conductivity of NG and ANG nanoparticles increases with frequency and thickness of NG and ANG pellets due to the conductive nature. Electrical conductivity and dielectric permittivity of NG and ANG are found to highly rely on thickness, according to the dielectric evaluation.

ARTICLE HISTORY
Received 17 December 2022
Accepted 11 August 2023

KEYWORDS
Synthesis; nano-graphite; spectroscopy; dielectric; permittivity; conductivity

1. Introduction

The development of surface modification of NG through oxidative modification is one of the most successful techniques. Many oxidizing materials including $KClO_3$ and fuming HNO_3, concentrated H_2SO_4 and HNO_3, a mixture of $NaNO_3$ and $KMnO_4$ in concentrated H_2SO_4 have been used in the literature, the surface of NG powder undergoes oxidative alteration, resulting in defect sites that are stabilized by covalently attaching different oxygen functional groups such carbonyls (–CO), carboxylic acids (–COOH), and hydroxyl groups (OH) [1–5]. The conductivity, tensile strength, and elasticity of composite materials can be improved by applying modified NG to various types of polymers and

CONTACT Shyama Prasad Mahapatra spmahapatra.chy@nitrr.ac.in

other substances. They can be utilized as electrode material for double-layer capacitors, superior electronic devices, batteries and capacitors [6–9]. To store more electrical energy, capacitors use dielectric materials with high permittivity and low losses [10,11]. Graphite is one of the most well-known allotropes of carbon and has a layered, planar construction. The graphene consists of bound of carbon sheets by weak van-der-Waal forces having 3.36 Å d spacing between the layers. Graphene has been a promising candidate for a number of applications, including photovoltaic, catalysis, nano-electronic, and energy storage and conversion [12–14], because of its peculiar two-dimension structure and superior optical, thermal, mechanical, and electrical capabilities. Microelectronics for large-scale power applications and energy storage devices are made from dielectric materials [15].

According to Lyddane–Sachs–Taller, lattice vibrations shift the intrinsic dipole moment, resulting to a very high permittivity [16]. Few publications on the dielectric examination of graphene oxide or graphene-based materials composites have been published in the literature [17,18]. Verdejo et al. demonstrated that the dielectric permittivity can be satisfactorily increased by homogeneously dispersing graphene oxide throughout the polymer cross-section [19]. The scotch-tape method and epitaxial chemical vapors deposition were the first methods used to create graphene nanosheets from bulk graphite [20,21]. By exfoliating graphite with potent oxidizing agents, NG and ANG are most frequently produced [22].

In the present study, NG powder was synthesized from graphite powder and its surface was modified using a strong acid mixture (sulphuric acid and nitric acid). SEM, HR-TEM, and XRD analysis of NG and ANG were performed to investigate the morphological structure. The functional group of modified NG was determined using FTIR spectroscopy. The dielectric relaxation of NG and ANG pellets were studied for usage in different fields. This included executing measurements of capacitance, dielectric permittivity, electrical conductivity, and dielectric loss tangent.

2. Experimental

2.1. Chemicals

Graphite powder, conc. HNO_3, conc. H_2SO_4, C_2H_5OH and other chemicals required were procured from the standard supplier.

2.2. Preparation of nano-graphite

First, a microwave synthesizer was used to irradiate graphite powder for 15 min at 200 °C and 10 psi. Irradiated graphite powder (2.0 g) was dissolved in a 7:3 volume ratio 100 mL mixture of de-ionized (DI) water and C_2H_5OH, and the mixture was then ultrasonically processed for 8–10 h. To obtain the NG powder, the precipitate was then filtered, rinsed with Millipore water using a centrifuge to remove any excess alcohol, and dried at 120 °C for 24 h in a vacuum oven.

2.3. Preparation of acid modified nano-graphite

The acid treatment of the synthesized NG was carried out using 100 mL of 1:3 combination of conc. H_2SO_4 and HNO_3. The mixed liquid was stirred for a few minutes before

being ultra-sonicated for 8 h. The liquid was neutralized to pH = 7 by adding de-ionized water. Finally, the acid-treated NG powder was extracted from the precipitate using a centrifuge, and then dried in a vacuum oven at 120 °C for 24 h to obtain ANG powder.

3. Measurements

3.1. Characterization techniques

The SEM (ZEISS EVO-50, Germany) was used to study the morphological properties of prepared NG and ANG powder. The HR-TEM (JEOL 2100, Japan) was used for measurement of particle sizes of the prepared NG and ANG. FTIR spectroscopy (Bruker Scientific Instrument, US) was used to study the functional groups of NG and ANG. The crystal structure of prepared NG and ANG was verified using XRD (XPert Pro PANalytical, Netherland). The dielectric relaxation spectra (DRS) of NG and ANG pellets in the 10^{-2}–10^{5} Hz frequency range were analyzed using the Hi-Tester LCR meter, Hioki 3533. From dielectric measurements, electrical conductivity has been evaluated according with the following relationship:

$$\sigma_{AC} = \omega\varepsilon_0\varepsilon' \tan\delta \quad (1)$$

where ω is $2\pi f$ (f is frequency), ε' is dielectric constant (C_p/C_0), ε_0 is vacuum permittivity and *tan* δ is the dielectric loss tangent [23].

4. Results and discussion

4.1. Scanning electron microscopy

The morphology of prepared NG and ANG have been studied through SEM with high vacuum mode in working distance at 8.5 mm and 20 kV. SEM image of NG and ANG are shown Fig. 1(a,b). From the Fig. 1(a), it is observed that NG shows an unclear surface folded thin sheet structure and Fig. 1(b) shows the crumpled and kinked structure due to presence of acid groups in surface of ANG.

4.2. High resolution transmission electron microscopy

High-power sonication reduces the thickness of the graphite structure up to significant level, as evidenced by interference microscope images. The particle sizes of prepared NG and ANG have been studied through HR-TEM. HR-TEM images of prepared NG and ANG is shown in Fig. 2(a,b). From the HR-TEM images, it can be observed that NG and ANG are in the range between 1 and 50 nm. The ANG also had more wrinkled and thin seat structures, indicating the presence of oxygen-containing functional groups.

4.3. Fourier-transform infrared spectroscopy

The different functional groups of acid-modified NG were studied through FTIR spectroscopy. The machine generated FTIR data of ANG is shown in Figure 3. The results

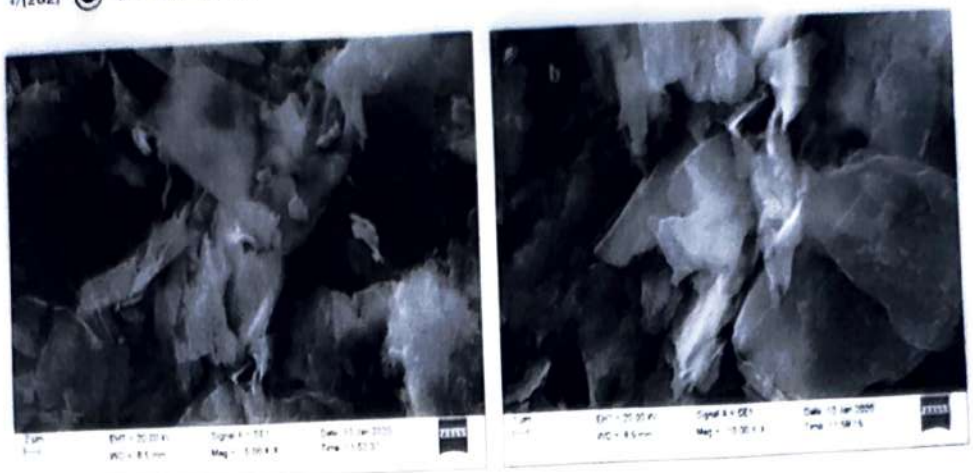

Figure 1. SEM image of (a) NG and (b) ANG.

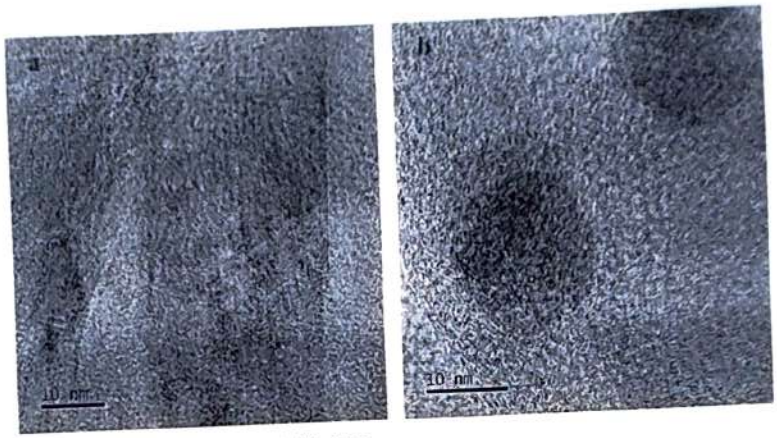

Figure 2. HR-TEM image of (a) NG and (b) ANG.

Figure 3. FTIR image of (a) NG and (b) ANG.

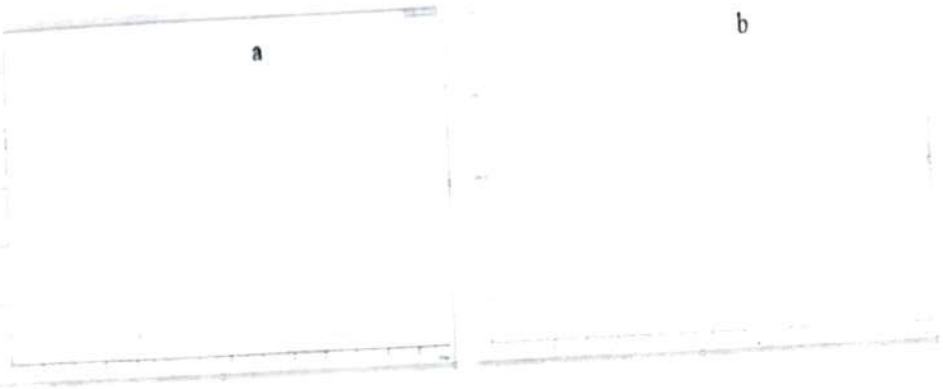

Figure 4. XRD image of (a) NG and (b) ANG.

demonstrated that in case of ANG, there are certain absorption peaks associated with distinct functional groups, however in the case of NG, there are none. Some absorption peaks at 3428.31 cm^{-1} due to O–H stretching vibration, while 1723.94 cm^{-1} represents the stretching frequency of carboxyl/carbonyl groups. The peak at 1632.00 cm^{-1} is responsible for the C=C stretching vibration. The peak at 1384.42 cm^{-1} is indicating the O–H group's bending vibration, while the peak at 1068.93 cm^{-1} is responsible for the stretching vibration of C–OH or C–O–C. The presence of all absorption peaks indicates that graphite powder in ANG has been successfully oxidized.

4.4. X-ray diffraction

The crystal structure of prepared NG and ANG was determined through XRD technique. The machine generated XRD spectra of prepared NG and ANG is shown in Fig. 4. NG and ANG show 2θ at 26.47° and FWHM is 1.9551 with 0.12 nm d-spacing which matches JCPDs no. is 75-2078 [24]. The Crystalline size of NG and ANG is 4.34 nm using the Scherer equation and Bragg equation [25]. The peaks have expanded and their intensity has diminished, suggesting a reduction in particle size, but there are no structural alterations.

$$Dp = (0.94 \times \lambda)/(\beta \times \mathrm{Cos}\theta) \tag{2}$$

where, β is the Line broadening in radians and Dp is the average crystallite size,

Bragg's equation:

$$n\lambda = 2d\sin\theta \tag{3}$$

where, λ is the X-ray wavelength, n is the diffraction series, θ is the Bragg angle, and d is the interlayer spacing.

4.5. Dielectric loss tangent

The dielectric loss tangent of prepared NG and ANG have been studied with frequency at different thickness (1, 2, 3, 5, and 7 mm) at room temperature as shown in Fig. 5(a,b). The tanδ increases with frequency at all thickness of NG and ANG pellets but this increase is not continuous after getting a peak it decreased with frequency due to

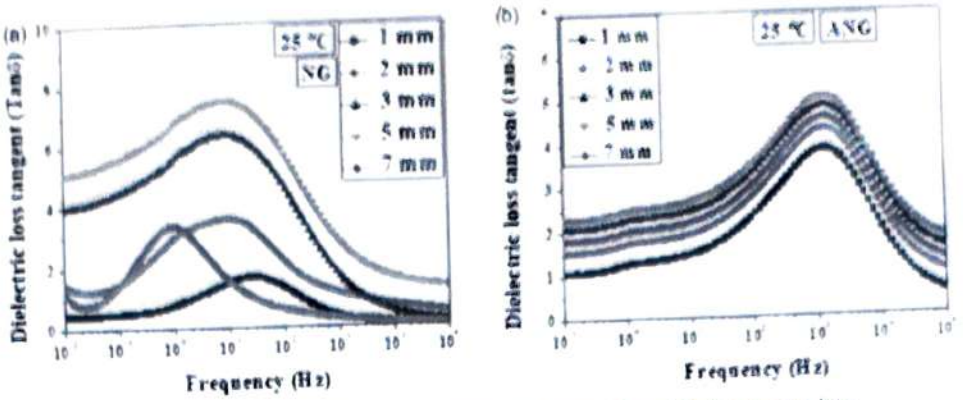

Figure 5. Dielectric loss tangent of (a) nano-graphite and (b) acid modified nano-graphite.

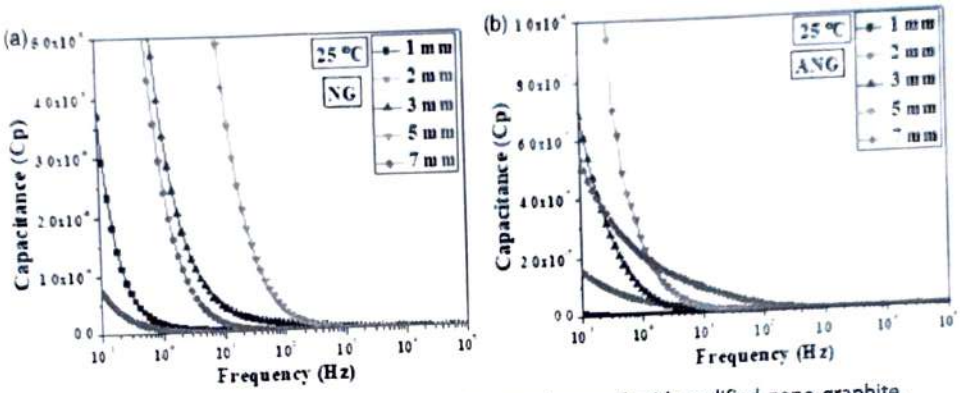

Figure 6. (a) Capacitance of nano-graphite and (b) capacitance of acid modified nano-graphite.

the presence of polar groups in the prepared ANG. It is also observed that the peak is shifting in case of ANG in presence of acid functional groups. The relaxation behavior of NG and ANG pellets depends mainly upon the thickness at room temperature. The maximum tan δ increases with the thickness of the NG and ANG pellets up to 5 mm this may be due to dipole relaxation and charge conduction developed [26] and decrease for 7 mm thickness, may be due to increase in resistivity and dipole fluctuation inside NG and ANG pellets [27].

4.6. Capacitance (Cp)

The variation in capacitance with frequency at different thicknesses (1, 2, 3, 5, and 7 mm) of synthesized NG and ANG nanoparticle is shown in Fig. 6(a,b) at room temperature. The capacitance decreases with frequency due to the orientation of functional groups of NG and ANG and increases with thicknesses due to capacitive nature of nanoparticles. From the figure, it is observed that the capacitance value increases with thickness up to 5 mm, and decreases for 7 mm thickness of the NG and ANG pellets, may be due to increase in resistivity inside NG and ANG pellets. As the frequency across a capacitor's pellets increases, the capacitor's capacitive reactance decreases. Therefore, the relationship between frequency and capacitive reactance is inverse. With

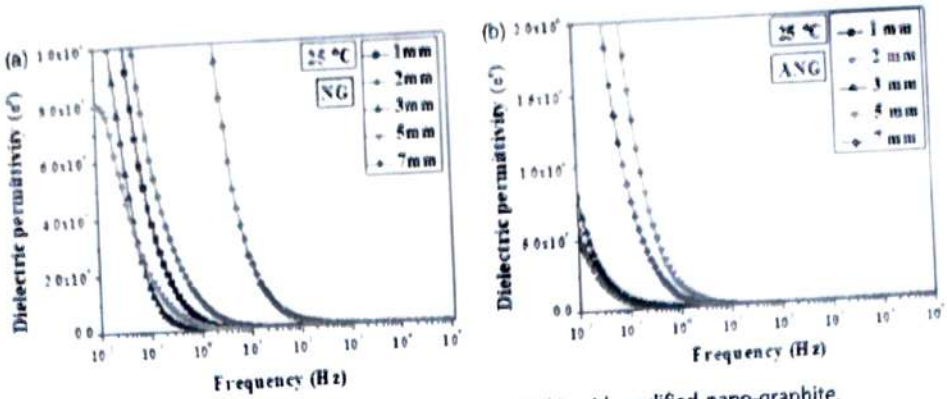

Figure 7. Dielectric permittivity of (a) nano-graphite and (b) acid modified nano-graphite.

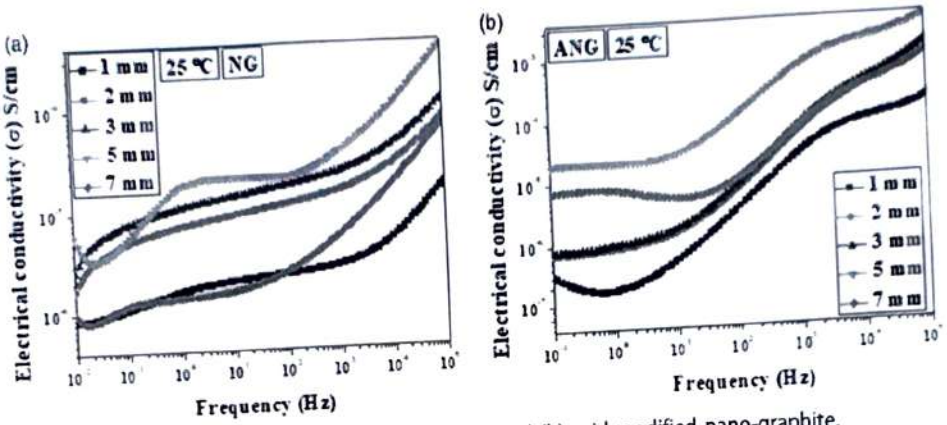

Figure 8. Electrical conductivity of (a) nano-graphite and (b) acid modified nano-graphite.

capacitive reactance's opposition to current flow, the electrostatic charge on the pellets (measured by their AC capacitance) does not change.

4.7. Dielectric permittivity (ε′)

The degree of electrical polarization of a material is revealed by the dielectric permittivity. The variation in dielectric permittivity with frequency at different thicknesses (1, 2, 3, 5, and 7 mm) of synthesized NG and ANG nanoparticle is shown in Fig. 7(a,b) at room temperature. The dielectric permittivity decreases with frequency and increase with thickness due to the charge orientation and dipole moment change of functional groups of modified NG [28,29]. From the figure, it can be observed that the dielectric permittivity increases with thickness of the NG and ANG pellets. The higher dielectric permittivity at low frequencies is may be due to the high electrical conductivity of NG and ANG and relating to ferroelectric nature of the conductive particles.

4.8. Electrical conductivity (σ)

The capacity to carry electrical current can be defined as electrical conductivity. The variation in electrical conductivity of NG and ANG pellets with frequency at different thicknesses are shown in Fig. 8(a,b). The electrical conductivity continuously increases

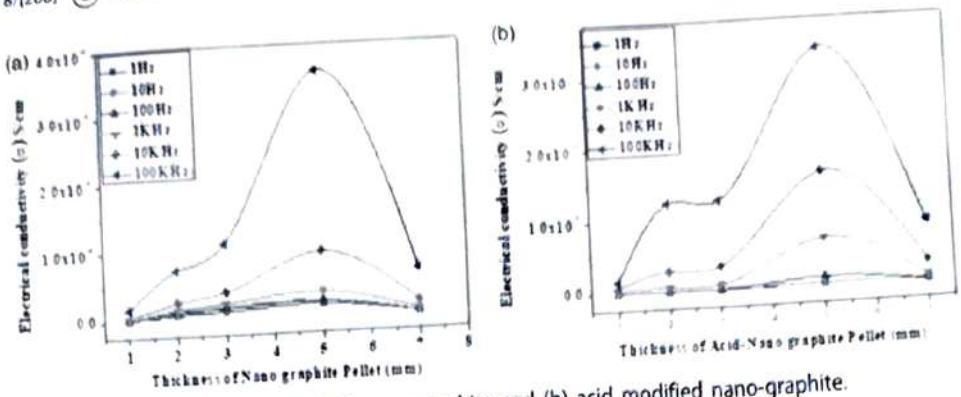

Figure 9. Percolation behavior of (a) nano-graphite and (b) acid modified nano-graphite.

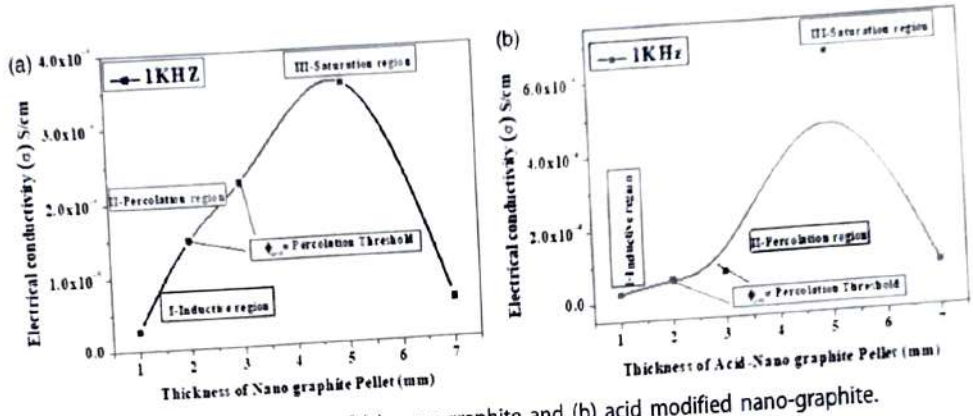

Figure 10. Electrical conductivity of (a) nano-graphite and (b) acid modified nano-graphite.

with frequency as well as thickness of NG and ANG pellets. From the figure, it is observed that the increasing electrical conductivity with thickness of NG and ANG pellet up to 5 mm as nanoparticle collisions create a continuous path for electrons to travel through the sample's volume. At 7 mm thickness, electrical conductivity is reduced may be due to formation of nanoparticle agglomerates and distortion of continuous path. Also, the decrease of electrical conductivity may be due to decrease in loss tangent and dielectric permittivity [30].

4.9. Percolation behaviour

The variation in percolation behavior of the electrical conductivity of NG and ANG pellets with thickness at different frequency (1, 10, 100 Hz and 1, 10, 100 kHz) is shown in Fig. 9. The electrical conductivity exponentially increases up to 5 mm thickness, after that decreases for 7 mm thickness of the NG and ANG pellet. This is may be due to the formation of nanoparticle agglomerates [31].

The electrical conductivity of NG and ANG pellets can be explained into three regions as given in Fig. 10. First region is an inductive region, electrical conductivity slowly increases with thickness as charge nanoparticles are smaller in number. Second region is a percolation region, electrical conductivity increase sharp due to the continuous conductive path formation and third region is saturation region, and an increasing

electrical conductivity is marginal effect or a decrease due to the agglomerates [32] formation of NG and ANG nanoparticle. The percolation thresholds have been identified between 4 and 5 mm thickness of NG and ANG pellet.

5. Conclusions

Nano-graphite and acid modified ANG nanoparticles have been prepared successfully from graphite powder by oxidation method. SEM images confirm surface morphology of NG, and ANG and HR-TEM study shows the nanoparticles NG and ANG are in the range of 1–50 nm. FTIR data confirmed the presence of acid functional groups on the surface of synthesized NG powder. XRD data of NG and ANG shows 2θ at 26.47° with an interlayer distance of 0.12 nm. The dielectric loss tangent spectra show relaxation peak with frequency and peak shifts due to presence of polar groups in the modified ANG. The capacitance values of NG and ANG decrease with frequency and increases with thicknesses due to the capacitive nature of nanoparticles. The decrease of capacitance for 7 mm thickness of the NG and ANG pellets may be due to the increase in resistivity of pellets. The dielectric permittivity decreases with frequency and increase with thickness may be due to the charge orientation and dipole moment change of functional groups of modified ANG. The higher dielectric permittivity at low frequencies is due to the ferroelectric nature of conducting nanoparticles. The electrical conductivity continuously increases with frequency as well as thickness of NG and ANG pellets. The electrical conductivity increases with thickness of NG and ANG pellet up to 5 mm which further decrease for 7 mm, may be due to decrease in loss tangent and dielectric permittivity. The percolation thresholds of NG and ANG pellets have been identified between 4 and 5 mm thicknesses. These results reveal that the NG and ANG nanoparticles are having an exciting possibility for high-dielectric based electrical applications, energy storage devices and sensors.

Acknowledgments

The authors thank the Director of the National Institute of Technology in Raipur for providing facility and support. Bhanu Pratap Singh, research scholar, additionally expresses thanks to the University Grant Commission (UGC), India, for providing financial support as a UGC-JRF.

Disclosure statement

No potential conflict of interest was reported by the authors.

ORCID

S. P. Mahapatra http://orcid.org/0000-0001-6949-5521

References

[1] B. C. Brodie, On the atomic weight of graphite, *Philos. Trans. R. Soc.* **249** (149), XIII (1859). DOI: 10.1098/rstl.1859.0013.

[2] L. Staudenmaier, Verfahren zur darstellung der graphitsäure, *Ber. Dtsch. Chem. Ges.* **31** (2), 1481 (1898). DOI: 10.1002/cber.18980310237.

[3] W. S. Hummers and R. E. Offeman, Preparation of graphitic oxide, *J. Am. Chem. Soc.* **80** (6), 1339 (1958). DOI: 10.1021/ja01539a017.

[4] C. Yu, C. F. Wang, and S. Chen, Facile access to graphene oxide from ferro-induced oxidation, *Sci. Rep.* **6**, 17071 (2016). DOI: 10.1038/srep17071.(2016).

[5] D. C. Marcano *et al.*, Improved synthesis of graphene oxide, *ACS Nano.* **4** (8), 4806 (2010). DOI: 10.1021/nn1006368.

[6] L. Dou *et al.*, Solution-processed copper/reduced-graphene-oxide core/shell nanowire transparent conductors, *ACS Nano.* **10** (2), 2600 (2016). DOI: 10.1021/acsnano.5b07651.

[7] T. Hsu *et al.*, Mesoscale characterization of local property distributions in heterogeneous electrodes, *J. Power Sources* **386**, 1 (2018). DOI: 10.1016/j.jpowsour.2018.03.025.

[8] A. Schönhals, and F. Kremer, Theory of dielectric relaxation, *Broadband Dielectric Spectrosc.* **1**, 59 (2003). DOI: 10.1007/978-3-642-56120-7_3.

[9] P. Kumar *et al.*, Dielectric properties of graphene oxide synthesized by modified hummers' method from graphite powder, *Integr. Ferroelectr.* **202** (1), 41 (2019). DOI: 10.1080/10584587.2019.1674822.

[10] Y. Wu *et al.*, Graphene/boron nitride–polyurethane microlaminates for exceptional dielectric properties and high energy densities, *ACS Appl. Mater. Interfaces.* **10** (31), 26641 (2018). DOI: 10.1021/acsami.8b08031.

[11] C. C. Homes, and T. Vogt, Doping for superior dielectrics, *Nat. Mater.* **12** (9), 782 (2013).), DOI: 10.1038/nmat3744.

[12] X. Hao, A review on the dielectric materials for high energy-storage application, *J. Adv. Dielect.* **3** (01), 1330001 (2013). DOI: 10.1142/S2010135X13300016.

[13] L. He *et al.*, First-principles study of the structure and lattice dielectric response of $CaCu_3Ti_4O_{12}$, *Phys. Rev. B* **65** (21), 214112 (2002). DOI: 10.1103/PhysRevB.65.214112.

[14] Y. Gao, and P. Hao, Mechanical properties of monolayer graphene under tensile and compressive loading, *Physica E Low Dimens. Syst. Nanostruct.* **41** (8), 1561 (2009). DOI: 10.1016/j.physe.2009.04.033.

[15] C. Berger *et al.*, Electronic confinement and coherence in patterned epitaxial graphene, *Science* **312** (5777), 1191 (2006).), DOI: 10.1126/science.1125925.

[16] S. Stankovich *et al.*, Graphene-based composite materials, *Nature* **442** (7100), 282 (2006). DOI: 10.1038/nature04969.

[17] Y. Sun *et al.*, Graphene based new energy materials, *Energy Environ. Sci.* **4** (4), 1113 (2011). DOI: 10.1039/C1EE01659H.

[18] Y. Liu *et al.*, Biological and chemical sensors based on graphene materials, *Chem. Soc. Rev.* **41** (6), 2283 (2012). DOI: 10.1039/C1CS15270J.

[19] W. Hu *et al.*, Electron-pinned defect-dipoles for high-performance colossal permittivity materials, *Nat. Mater.* **12** (9), 821 (2013). DOI: 10.1038/nmat3691.

[20] T. Ramanathan *et al.*, Functionalized graphene sheets for polymer nanocomposites, *Nat. Nanotechnol.* **3** (6), 327 (2008). DOI: 10.1038/nnano.2008.96.

[21] D. A. Dikin *et al.*, Preparation and characterization of graphene oxide paper, *Nature* **448** (7152), 457 (2007). DOI: 10.1038/nature06016.

[22] L. J. Romasanta *et al.*, Functionalised graphene sheets as effective high dielectric constant fillers, *Nanoscale Res. Lett.* **6**, 1 (2011). DOI: 10.1186/1556-276X-6-508.

[23] F. Kremer, and A. Schönhals, (Eds.). 2002 *Broadband Dielectric Spectroscopy*. Springer Science & Business Media, Berlin Heidelberg.

[24] A. Shalaby *et al.*, Structural analysis of reduced graphene oxide by transmission electron microscopy, *Bulg. Chem. Commun.* **47**, 291 (2015).

[25] J. Li *et al.*, The preparation of graphene oxide and its derivatives and their application in bio-tribological systems, *Lubricants* **2** (3), 137 (2014). DOI: 10.3390/lubricants2030137.

[26] M. T. Sebastian *et al.*, Measurement of microwave dielectric properties and factors affecting them, *Microwave Mater. Appl. 2V Set* **1**, 1 (2017). DOI: 10.1002/9781119208549.ch1.

[27] P. Kumar *et al.*, Synthesis and dielectric relaxation spectroscopy of graphene oxide nanoparticles: effects of frequency, thickness, and temperature, *J. Elec. Mater.* **49** (10), 5801 (2020). DOI: 10.1007/s11664-020-08355-9.

[28] J. Saji *et al.*, Impedance and dielectric spectroscopy of nano-graphite reinforced silicon elastomer nanocomposites, *Fibers Polym.* **16** (4), 883 (2015). DOI: 10.1007/s11664-020-08355-9.

[29] S. K. Tiwari *et al.*, Dynamic mechanical and dielectric relaxation studies of chlorobutyl elastomer nanocomposites: Effect of nanographite loading and temperature, *High Perform Polym.* **27** (3), 274 (2015). DOI: 10.1177/0954008314545137.

[30] P. S. Das *et al.*, Electrical properties of $Li_2BiV_5O_{15}$ ceramics, *Physica B* **395** (1-2), 98 (2007). DOI: 10.1016/j.physb.2007.02.065.

[31] D. Xu *et al.*, Dielectric properties of exfoliated graphite reinforced flouroelastomer composites, *J. Appl. Polym. Sci.* **111** (3), 1358 (2009). DOI: 10.1002/app.29183.

[32] M. Nanda *et al.*, Dielectric relaxation of conductive carbon black reinforced chlorosulfonated polyethylene vulcanizates, *Polym. Compos.* **1**, 152 (2010). DOI: 10.1002/pc.20779.